



**HAL**  
open science

## Hydraulic Turbine Vortex detection and visualization using Strain Gauge Sensor

Irina Murgan, Gabriel Vasile, Cornel Ioana, Stéphane Barre, Thierry  
Lora-Ronco

► **To cite this version:**

Irina Murgan, Gabriel Vasile, Cornel Ioana, Stéphane Barre, Thierry Lora-Ronco. Hydraulic Turbine Vortex detection and visualization using Strain Gauge Sensor. IEEE Sensors Letters, 2017, pp.1 - 1. 10.1109/LSENS.2017.2750402 . hal-01592678v1

**HAL Id: hal-01592678**

**<https://hal.science/hal-01592678v1>**

Submitted on 25 Sep 2017 (v1), last revised 5 Oct 2017 (v2)

**HAL** is a multi-disciplinary open access archive for the deposit and dissemination of scientific research documents, whether they are published or not. The documents may come from teaching and research institutions in France or abroad, or from public or private research centers.

L'archive ouverte pluridisciplinaire **HAL**, est destinée au dépôt et à la diffusion de documents scientifiques de niveau recherche, publiés ou non, émanant des établissements d'enseignement et de recherche français ou étrangers, des laboratoires publics ou privés.

# Hydraulic Turbine Vortex detection and visualization using Strain Gauge Sensor

Irina Murgan<sup>1</sup>, Gabriel Vasile<sup>1\*</sup>, Cornel Ioana<sup>1\*\*</sup>, Stéphane Barre<sup>2</sup>, Thierry Lora-Ronco<sup>3</sup>

<sup>1</sup> GIPSA-lab, Université Grenoble Alpes, 11 rue des Mathématiques BP 46, Saint Martin d'Hères, Grenoble, France

<sup>2</sup> LEGI, UMR 5519, Grenoble, France

<sup>3</sup> EDF-DTG, Grenoble, France

\* Senior Member, IEEE

\*\* Member, IEEE

**Abstract**—Hydraulic machinery monitoring using non-intrusive sensors is today's trend in the hydroelectric power industry. The phenomena of cavitation vortex occurs mostly at off-design regimes, which reduces the turbine's efficiency. In this paper we propose a mathematical model for vortex detection and a 3D vortex presence visualization. Its visualization is constructed on the gyroscope principle, translating the strain gauge vertical elongations into a nutation movement. The mathematical model for vortex detection computes the data statistical moments. The model is tested on experimental data recorded using an extensometer.

**Index Terms**—extensometer, hydraulic turbine monitoring, pdf estimation, vortex detection

## I. INTRODUCTION

Rotating machines, such as rotary engines, turbines or wheels, are often exposed, during their operational lifetime to several undesired phenomenon: vibrations, mechanical stress or cavitation [1]. Such phenomena can lead to premature wear of the machines or worse, to their destruction [2]. It is particularly the case for the hydraulic turbines, because of their dimensions, diversity and components complexity.

A hydraulic turbine is mainly composed by a specific number of guide vanes that control the water flow rate, the moving part (rotor-blade assembly), the draft tube controlling the water evacuation and the electrical generator that transform the mechanical energy into electrical energy. The turbine is designed to transform the water kinetic energy with maximum of efficiency, under certain operating conditions, called best efficiency operating point.

Nowadays, the expansion of renewable energy sources (solar, wind, etc.) may affect, by their intermittent nature, the stability of the power system. In order to maintain the balance between energy production and consumption, the hydroelectric power plants are often used. Thus, in order to be able to respond to a various demands of the power grid, the hydraulic turbines tend to have their operation range extended (i.e. operate under off-design conditions). When a hydraulic turbine operates under off-design conditions, the phenomena of vortex cavitation is likely to appear [3]. The conditions for vortex cavitation appearance are an unsteady flow with water pressure drop under the water vaporization pressure. In this case, the turbine efficiency is decreased as flow instabilities induce mechanical vibrations and large pressure fluctuations. They generate axial and radial efforts together with the mechanical stress created by the turbine's rotation. Apart from the machine mechanical damage, output power fluctuations are

generated, putting at risk the electrical grid stability. Therefore, it is important to know at every instance of time, the amplitude of these instabilities and to be able to control them. Up to a certain level, the efforts are absorbed by a coupling system composed by bearings, thus avoiding a direct transfer to the electrical generator. In today practice, for hydraulic system monitoring, intrusive pressure sensors are used in order to detect pressure fluctuations. Mathematical simulations and reduce scale tests are also performed for flow prediction and vortex identification [4-9]. Due to flow instabilities and turbulences, these methods cannot be generalized, despite that they may provide satisfying results [10-12].

Multiple sensors of different types are used in order to perform constant hydropower plant monitoring, especially in the case of the rotational components. In particular, the time evolution of the axial efforts is measured using extensometers. Having the extensometer elongations measurements at the bearing unit level, we propose a novel processing method, in order to visualize the turbine off-design behavior in terms of the generated axial efforts. Our study is based on a mathematical model, presented in section II of this paper. In section III, the model is applied to a real calibration dataset, for different turbine's operating conditions. Conclusions and perspectives are presented in section IV.

## II. THEORETICAL FRAMEWORK

In order to characterize the vortex cavitation presence, we create a mathematical and statistical interpretation of the generated axial efforts. The proposed method performs a conversion of the measured elongations in a way that the axial efforts can be directly interpreted with the nutation movement of a gyroscope (Fig. 1). This axial effort's measurement is crucial in quantifying the instabilities levels at the current operational point of the turbine. Similar representations are

performed in [13], as part of shaft dynamical analysis. The analogy between the extensometer measurements and the nutation movement provides a new virtual monitoring instrument of the machine instabilities. In the proposed framework we expect to obtain a minimum level of instabilities for the best efficiency point, and larger one for lower efficiency operating points.

### A. Mathematical model

Let consider a circle,  $C$ , in a spherical coordinates system  $(r, \varphi, \theta)$ , to which we apply a set of three rotation matrixes,  $R_x$ ,  $R_y$  and  $R_z$ , for each of the three directions x, y respectively z. The rotated circle,  $C_r$ , is given by the following system of equations:

$$C_r = R_z \times R_x \times R_y \times C, \quad (1)$$

Here,  $t \in [0, T]$ , with  $T$  being the duration of one full rotation of a disk around the  $Oz$  axis and  $\varphi, \theta \in [0, 2\pi]$ . We define the rotation angle  $\varphi$  as a function of the extensometer elongations measurements,  $S_{in}(t)$ :

$$\varphi(t) = \arctg\left(\frac{S_{in}(t)}{r}\right) \quad (2)$$

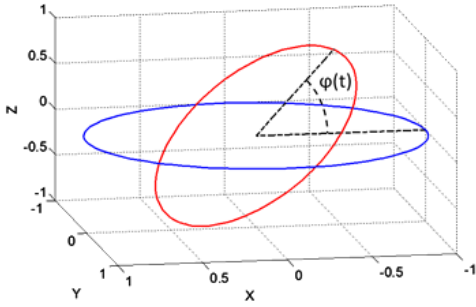


Fig. 1. 3D rotation of a circle with angle  $\varphi$ , around y-direction.

Let us consider a nonlinear operator:  $X$ . If the  $X$  operator is applied to our signal  $S_{in}(t)$ , the response is given by:

$$X\{S_{in}(t)\} = \frac{1}{1 + S_{in}^2(t)} \quad (3)$$

We rewrite the equations system (1) as follows:

$$C_r = r \cdot \begin{pmatrix} \sin[\theta(t)] & \cos[\theta(t)] & -\sin[\theta(t)] \\ \cos[\theta(t)] & \sin[\theta(t)] & \cos[\theta(t)] \\ 0 & -\sin[2\varphi(t)] & \sin[\varphi(t)] \end{pmatrix} \cdot \begin{pmatrix} \cos[\alpha(t)] & 0 & -\cos[\alpha(t)] \\ 0 & \cos[\alpha(t)] & 0 \\ 0 & \sin[\alpha(t)] & 0 \end{pmatrix} \cdot \begin{pmatrix} \cos^2[\varphi(t)] \\ \cos[\varphi(t)] \\ 1 \end{pmatrix} =$$

$$= r \cdot M(t) \cdot \begin{pmatrix} \cos^2[\varphi(t)] \\ \cos[\varphi(t)] \\ 1 \end{pmatrix} \stackrel{r=1}{\Leftrightarrow} M(t) \cdot \begin{pmatrix} X\{S_{in}(t)\} \\ (X\{S_{in}(t)\})^{\frac{1}{2}} \\ 1 \end{pmatrix} \quad (4)$$

In (4), the unity circle is considered. Further, we will study the response of different types of input signals, when we will apply the proposed operator  $X$ . The input signal pattern is: a steady state component,  $s(t)$  (which corresponds to a deterministic process, in this case the turbine rotation frequency) and the additive noise:

$$S_{in}(t) = s(t) + n(t) \quad (5)$$

We have chosen to express in this way the signal pattern, because we will perform a statistical analysis later. Generally, the probability

density function for an experimental data can be predicted, if it has a Gaussian or sinusoidal shape [14]. Deterministic signals have periodic amplitudes that allow harmonically decomposition related to sin waves, thus  $s(t)$  will be the sin wave corresponding to the turbine rotation. The additive noise,  $n(t)$ , present in the frequency bandwidth which corresponds to the cavitation vortex, is assumed to be Gaussian.

In the following sections we will analytically estimate the response of each component, sinusoid and noise, to the  $X$  operator.

### B. Gaussian noise input

Let us consider the case of independent and identically distributed Gaussian noise input,  $n(t)$ . The corresponding probability density function, pdf, is given by the following relation:

$$p_n(x) = \frac{1}{\sigma\sqrt{2\pi}} e^{-\frac{(x-\mu)^2}{2\sigma^2}}, \quad -\infty < x < \infty \quad (5)$$

We want to see how  $p_n(x)$  is changed if we apply the  $X$  operator. We will perform a probability density function variable change [11]. Let's consider a random and continuous variable  $x$ , normally distributed, with the probability density function given by (6). The variable change that we propose is:  $x \rightarrow \frac{1}{1+x^2}$ . Hence, consider the function  $X_n(x) = \frac{1}{1+x^2}$  which is strictly increasing on the interval  $(-\infty, 0]$  and strictly decreasing on the interval  $[0, \infty)$ . On both intervals,  $X_n$  is continuous and differentiable.

The equation  $X_n(x) = y$  has the following two solutions:

$$x_1 = \sqrt{\frac{1-y}{y}} \quad \text{and} \quad x_2 = -\sqrt{\frac{1-y}{y}}.$$

Thus, we have:

$$p_n(y) = \frac{p_n(x_1)}{|X'_n(x_1)|} + \frac{p_n(x_2)}{|X'_n(x_2)|} =$$

$$= \frac{1}{\sigma y \sqrt{2\pi y(1-y)}} \cdot \left[ e^{-\frac{(\sqrt{\frac{1-y}{y}} - \mu)^2}{2\sigma^2}} + e^{-\frac{(-\sqrt{\frac{1-y}{y}} - \mu)^2}{2\sigma^2}} \right] \quad (6)$$

for  $y \in (0,1)$ . An example of the estimated and calculated  $X$  transform of a Gaussian noise pdf is displayed in Fig. 2. According to (7), the pdf domain of definition is restrained to the interval  $(0, 1)$ .

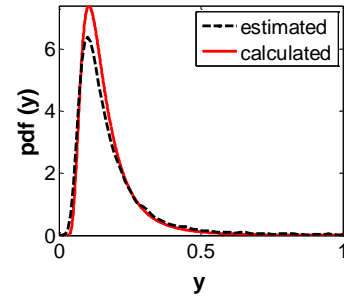


Fig. 2. Probability density function of the  $X$  transform of a Gaussian noise  $\sim N(2.5, 0.5)$  has the mean=0.15 and the variance=0.01 if it is computed using (7), and it has the mean=0.17 and the variance=0.3 if it is numerical estimated.

### C. Sinusoidal with additive noise input

In this section, we will perform the pdf analysis of the  $X$  transform of a sinusoidal wave with Gaussian noise. Consider a sinusoidal wave of the form:  $s(t) = A \cdot \sin(2\pi ft + \theta)$ . Firstly, we compute the joint pdf of one sinusoid and an additive noise, supposed to be Gaussian noise. It is given by the convolution of their corresponding pdfs [14]:

$$p_{S_{in}}(x) = \int_{-\infty}^{\infty} p_s(x - \tau) * p_n(\tau) d\tau \quad (7)$$

$$= \frac{1}{\sigma\pi\sqrt{2\pi}} \int_0^{\pi} e^{-\left(\frac{x - A\cos(\theta)}{4\sigma}\right)^2} d\theta$$

where  $\sigma$  is the noise's standard deviation;  $A$  and  $\theta$  are the sinusoidal wave's amplitude and phase. If we develop, in Taylor- MacLaurin series, the exponential term from (8), then  $p_{S_{in}}(x)$  can be rewritten as follows:

$$p_{S_{in}}(x) = \frac{\alpha}{\sigma\sqrt{2\pi}} e^{-\left(\frac{x}{4\sigma}\right)^2} \quad (8)$$

where  $\alpha = \alpha(A, \sigma, N)$  is a constant depending on the sinusoid amplitude, noise standard deviation and the number of Taylor- MacLaurin series terms,  $N$ . For calculus simplicity, we suppose  $N$  is an odd number.

Secondly, we perform for  $p_{S_{in}}(x)$  the same variable change as in the previous section, and we will get the pdf of  $X(S_{in})$ :

$$p_{X(S_{in})}(y) = \frac{\alpha}{\sigma\sqrt{2\pi}y^3(1-y)} \cdot e^{\frac{y-1}{(4\sigma)^2y}} \quad (9)$$

The  $k$ -th order moments of  $p_{X(S_{in})}(y)$ ,  $k \geq 1$ , are given by the following relation [15]:

$$m_k = \int_{-\infty}^{\infty} y^k \cdot p_{X(S_{in})}(y) \quad (10)$$

As mentioned in previous section,  $y \in (0,1)$ . We perform the variable change  $\frac{1-y}{y} = t$  and we obtain:

$$m_k = \frac{\alpha}{\sigma\sqrt{2\pi}} \int_0^{\infty} \frac{1}{\sqrt{t}} \cdot \frac{1}{(1+t)^k} \cdot e^{-at} dt \quad (11)$$

with  $a = \frac{1}{(4\sigma)^2}$ . If we compute the integral from (12), for the first moment [16], we get:

$$m_1 = \pi \cdot \frac{\alpha}{\sigma\sqrt{2\pi}} \cdot e^a \cdot \text{erfc}(\sqrt{a}) \quad (12)$$

As Eq. (12) proves, the pdf's moments are functions of sinusoid amplitude and noise standard deviation. The sinusoid describes a deterministic process, hence  $A$  is known, and  $\sigma$  can be estimated.

In order to test the robustness of our proposed transform, we perform an SNR level test. The moments of first and second order are calculated for a SNR range between -30 and 10 dB. Their variation is displayed in Fig. 3.

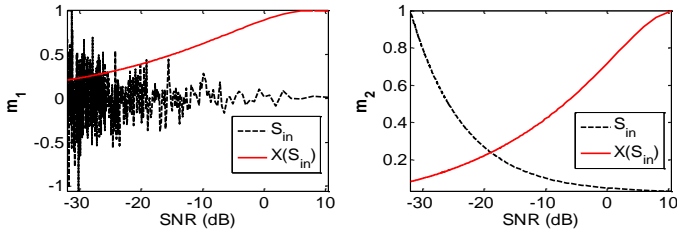


Fig. 3. SNR level test.

### III. Experimental tests and results

#### A. Data acquisition

In our experiment, SCAIME Epsimetal extensometer sensor with a resolution better than  $1\mu\text{m/m}$  [17] is placed on the alternator bearing conical support at 150mm distance from its outer edge and at 300mm distance from the alternator bearing of a Francis turbine (Fig. 4).

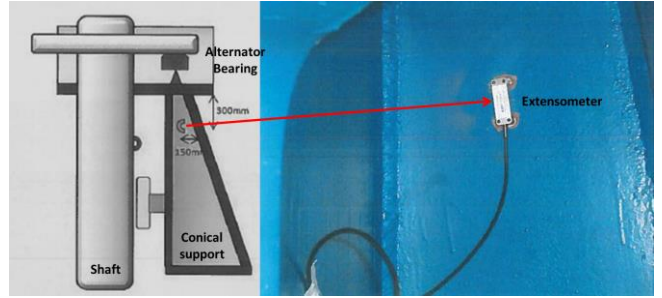


Fig. 4. The extensometer placement on the alternator bearing.

Using 18 different operating conditions (different water flow rates, between 80 and 350 l/s), elongations variations were recorded with a sampling rate of 5120 Hz. The extensometer measurements are related to the turbine mechanical behavior. The link with the hydraulic phenomenon is made by the presence of low frequencies, under 1Hz, in the spectral analysis of the recorded data.

#### B. Results

The theoretical framework presented in part II, will be used now to detect and visualize the cavitation vortex presence (Fig. 5). The input signal,  $S_{in}(t)$ , is composed by the sum of one sinusoids, corresponding to the turbine rotation frequency and the noise in the corresponding vortex frequency bandwidth: between 0.5 and 1 Hz.

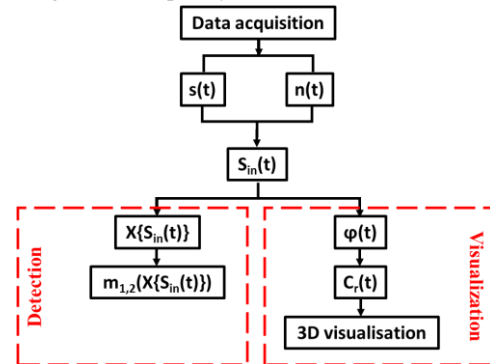


Fig. 5. Measured data processing method.

The vortex detection is performed by the computing the first and second order statistical moments of  $S_{in}$  and  $X\{S_{in}\}$ , for several working regimes. In order to apply (12), the sinusoid parameters are constants, no matter the turbine's working regime, and  $\sigma$  is the reference noise standard deviation (the  $\sigma$  of recorded noise for the optimal working conditions of the turbine). Fig. 6 shows moments variation of  $S_{in}$  and  $X\{S_{in}\}$ , for all flow rates. The effect of using the proposed transform  $X$ , is that the statistical moments  $m_1$  and  $m_2$  of  $X\{S_{in}\}$  are correlated and they vary according to the cavitation vortex appearance.

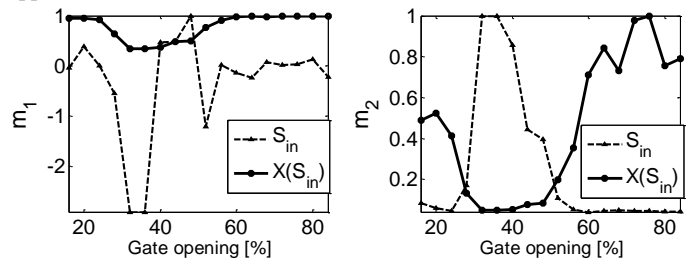


Fig. 6. Statistical moments variation as a function of the gate opening.

One can notice a vortex detection event by the drop of the second order moment,  $m_2$ , for a gate opening between 25-50%. The vortex presence, hence appearance of its corresponding frequency, is marked by a lower data's second order moment. The first order moment do not provide enough information, especially that of  $S_{in}$ . Using (3), the extensometer's vertical elongations are transposed to angular rotation of a circle with 3 degree of freedom: rotation around  $x$ ,  $y$  and  $z$  directions. In order to obtain a 3D rotation of the circle, at every instance of time, a product of the three rotation matrices following (1) and (2), for each direction, is applied to a unitary circle in initial position. The rotation period is equal to the vortex rotation period. Eq. (4) gives the spherical coordinates of the rotated circle, at each time instant  $t$ . In Fig. 7 we can visualize, on the turbine hill chart, the presence of the cavitation vortex. Three operating points are considered: part load (PL), the best efficiency point (BEP) and high load (HL). For PL, more than for HL, the vortex appearance is marked by the presence of low frequencies on signal's spectrogram, and by the deviation from the 3D circle reference position given by the BEP.

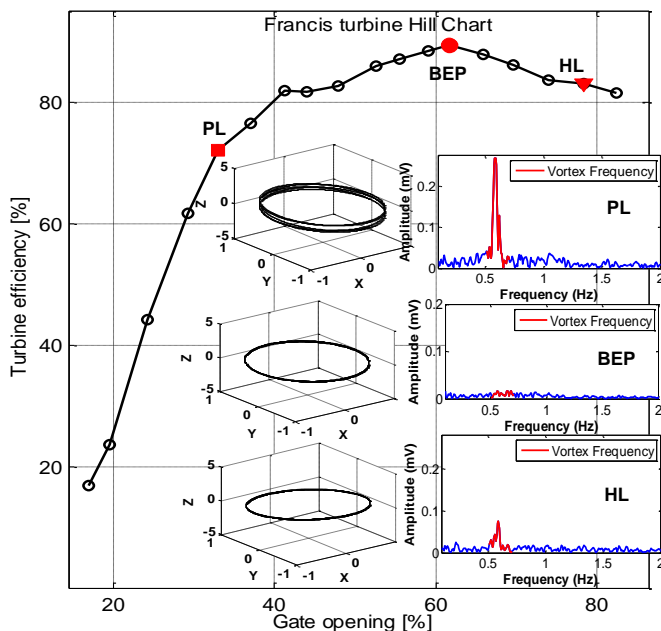


Fig. 7. 3D interpretation of the vortex cavitation appearance.

In the case of cavitation vortex appearance, the statistical moments of the corresponding signal are close to those of a Gaussian pdf. This fact is in agreement with our initial assumption from section II.A, that the additive noise present in the cavitation vortex frequency bandwidth is considered to be Gaussian.

#### IV. CONCLUSION

Cavitation vortex and all flow instabilities have a major impact on hydraulic machinery efficiency. The ability to detect instantly the flow parameters changes, improves the machines monitoring and thus, low efficiency exploitation can be avoided. In this paper we have presented a new application for extensometer measurements, which provide real time information about the cavitation vortex appearance, using a mathematical model for data processing. Perspectives of study concern the adaptive estimation for the reference noise standard deviation [18].

#### ACKNOWLEDGMENT

We would like to thank Mr. Jean-Louis Ballester for his recommendations and also to the “Électricité de France” (EDF) for providing the experimental calibration data.

#### REFERENCES

- [1] Landau L D and Lifschitz E M (1976), *Mechanics*, New York Pergamon, pp. 113.
- [2] Round G F (2004), *Incompressible flow turbomachines: design, selection, applications and theory*, Elsevier, Amsterdam, pp. 55-102.
- [3] Franc J P (2005), *Fundamentals of cavitation*, Springer Netherlands vol. 76, pp. 265.
- [4] Houde S, Iliescu M, Fraser R, Lemay S, Ciocan GD, Deschênes C (2011) “Experimental and Numerical Analysis of the Cavitating Part Load Vortex Dynamics of Low-Head Hydraulic Turbines”, *Fluids Engineering Division Summer Meeting, ASME-JSME-KSME, Joint Fluids Engineering Conference*, Vol. 2, For a ( ):171-182, doi:10.1115/AJK2011-33006.
- [5] Paik J, Sotiropoulos F, Sale MJ (2005), “Numerical simulation of swirling flow in complex hydroturbine draft tube using unsteady statistical turbulence models”, *Journal of Hydraulic Engineering*, Vol. 131, no. 6, pp. 441-456.
- [6] Susan-Resiga R, Ciocan GD, Anton I, Avellan F (2006), “Analysis of the swirling flow downstream a Francis turbine runner”, *Journal of Fluids Engineering*, Vol. 128, pp. 177-189 10.
- [7] Tridon S, Barre S, Ciocan GD, Tomas L (2010), “Experimental Analysis of the Swirling Flow in a Francis Turbine Draft Tube: Focus on Radial Velocity Component and Possible Applications Determination” - *European Journal of Mechanics – B/Fluids*, ISSN: 0997-7546, vol. 25, Issue 4, pp. 321-335.
- [8] Yuning Z, Kaihua L, Haizhen X, Xiaozhe D (2017), “A review of methods for vortex identification in hydroturbines”, *Renewable and Sustainable Energy Reviews*, <https://doi.org/10.1016/j.rser.2017.05.058>.
- [9] Wang X., Nishi M., Tsukamoto H., 1994, “A simple model for predicting the draft tube surge”, *Proceedings of the 17th IAHR Symposium*, vol. 1, pp. 95-106, Beijing, China, September 15-19.
- [10] Iliescu M (2007), *Analysis of large scale phenomena in turbine draft tubes*, Ph. D. dissertation, EPFL Lausanne, Switzerland.
- [11] Konidaris D N, Tegopoulos J A (1997), “Investigation of oscillatory problems of hydraulic generating units equipped with Francis turbines”, *IEEE Trans. on Energy Conversion*.
- [12] Hongqing F, Long C, Nkosinathi D, Zuyi S (2008), “Basic modeling and simulation tool for analysis of hydraulic transients in hydroelectric power plants”, *IEEE Trans. on Energy Conversion*.
- [13] Denis S (2014), *Analyse dynamique d'une ligne d'arbre verticale supportée par une butée à patins oscillants*, Ph. D. dissertation, University of Poitiers, France.
- [14] Chermisinoff N P (1987), *Practical Statistics for Engineers and Scientists*, Technomic Publishing Company, Pennsylvania, ISBN 87762-505-0, pp. 61-63.
- [15] Ventsel H (1973), *Théorie des probabilités*, Editions de Moscou, pp. 251-253.
- [16] Abramowitz M, Stegun I, (1964), *Handbook of mathematical functions with formulas, graphs and mathematical tables*, pp. 302.
- [17] Le Roux M, Vasile G, Lora-Ronco T, “Analyse de signaux issus de capteurs extensométriques de poussée hydraulique”, Internship report, <https://doi.org/10.13140/RG.2.2.26709.01768>.
- [18] Pastor D, Socheleau F (2012), “Robust estimation of noise standard deviation in presence of signals with unknown distributions and occurrences”, *IEEE Trans. on signal processing*, vol. 60, no. 4.